Springer

KSME

Journal of Mechanical Science and Technology 33 (12) (2019) 6063~6073
www.springerlink.com/content/1738-494x(Print)/1976-3824(Online)
DOI 10.1007/s12206-019-1150-z

Chemical, thermal and dilution effects of carbon dioxide in oxy-fuel combustion of wood in a fixed bed †

Josephat Kipyegon Tanui[1,*], Paul Ndirangu Kioni[1], Thomas Mirre[2] and Mario Nowitzki[2]

[1]*Department of Mechanical Engineering, Dedan Kimathi University of Technology, P.O. Box 657-10100, Nyeri, Kenya*
[2]*Fachbereich Ingenieur- und Naturwissenschaften, Technische Hochschule Wildau, Hochschulring 1, 15745 Wildau, Germany*

(Manuscript Received February 18, 2019; Revised September 20, 2019; Accepted October 10, 2019)

Abstract

Experimental and numerical modeling was performed on eucalyptus wood combustion under oxy-fuel conditions using a fixed bed reactor in order to isolate the role of various carbon dioxide effects on the burning rate. Wood combustion was investigated under four different mixtures of O_2 and $Ar/CO_2/N_2$: 21 % O_2/79 % N_2; 21 % O_2/22.5 % CO_2/56.5 % Ar; 40 % O_2/60 % CO_2; and 40 % O_2/47 % CO_2/13 % Ar. The first three mixtures were designed to have the same peak temperatures in order to isolate chemical and dilution effects of CO_2. This was achieved by substituting some percentage of CO_2 with Ar in O_2/CO_2 mixture while maintaining a constant concentration of O_2. The fourth mixture was meant to isolate the thermal effect of CO_2. The results were obtained from both the experimental rig and numerical simulation for a fixed bed configuration. Wood combustion in the fixed bed was modeled using Lagrange-Euler method, where gas-phase was calculated using computational fluid dynamics (CFD), that is Euler phase, while solid-phase was tracked in Lagrange phase using discrete element method (DEM). The results show that ignition time in CO_2 environment decreases gradually as O_2 concentration is increased. On the other hand, burning rate and flame front speed increase as O_2 concentration is increased. It was established that dilution effect is the most influential parameter on the burning rate of wood combustion in an oxy-fuel system.

Keywords: Burning rate; CO_2 effect; Fixed bed; Oxy-fuel combustion; Wood combustion

1. Introduction

The demand for biomass fuel has increased due to ever increasing energy need that cannot be fully satisfied by other energy sources, such as coal. Biomass is an attractive energy source as compared to coal as it is renewable. Most of the energy scenarios indicate that biomass will be increasingly used to meet increasing energy demand in future [1].

For a long time, biomass has been converted to energy using burners which operate under air-fuel conditions. However, in the last two decades, there has been increasing use of combustion of biomass in power generation [2, 3]. Oxy-fuel combustion is a technique of capturing CO_2 by recirculating exhaust gas. It is applicable to solid fuels [4], liquid fuels [5] and gaseous fuels [6]. The technique was introduced in power plants the first time in 1982 [7]. Since then, a lot of research, for instance [8-10], have been done to understand the combustion phenomenon.

The studies on fundamental combustion phenomena - transport, chemical and thermodynamics processes - occurring in oxy-fuel combustion are based on models and experiments on laboratory-scale devices. These include studies on ignition delay time in coal [11], ignition temperature, burnout and NO_x emission in biomass and coal blends [12], and gaseous emissions from biomass/coal co-firing [13]. Such studies provide insights into combustion phenomena in practical oxy-fuel environment [12, 13]. The presence of CO_2 in oxidizer alters physical and thermal properties of the gas mixture, which has impact on fuel reactivity, flame temperature and emissions. Unlike inert species such as argon and nitrogen which have only thermal and dilution effects on combustion processes, addition of reactive species such as CO_2 introduces a chemical effect [14, 15]. Dilution effect is the reduction of concentration of oxidizer caused by addition of CO_2, thermal effect is the decrease in temperature caused by addition of CO_2 and chemical effect is the direct active participation in the chemical reactions.

The three roles played by CO_2 addition can be separated by adjusting the flame temperature to a value corresponding to a reference condition without change in oxidizer and fuel relative concentrations [15, 16]. This technique has been applied to study the effects of CO_2 on soot formation, but it can also be applied to study the effects on other combustion properties [17].

*Corresponding author. Tel.: +254 723503095
E-mail address: josephat.tanui@dkut.ac.ke
† Recommended by Associate Editor Jeong Park
© KSME & Springer 2019

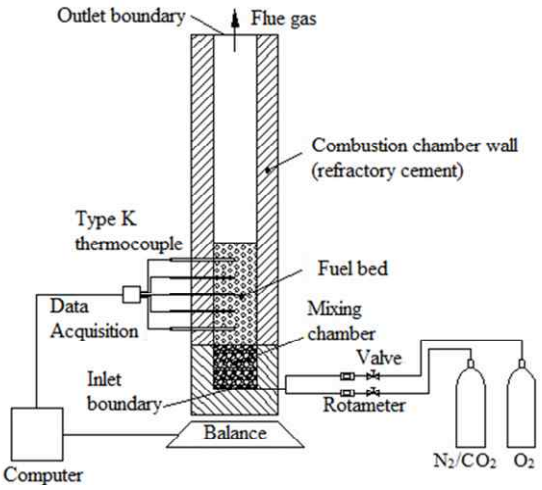

Fig. 1. Schematic diagram of experimental set-up.

Most previous studies focused on the overall effects of CO_2 burning environment on ignition time [18], ignition and combustion temperature [19], burnout [20], combustion intensity [19] and thermal reactivity [21]. The individual effects in terms of chemical, thermal and dilution on the combustion properties are still not clear. An understanding of these basic mechanisms through which CO_2 affects combustion processes is important because it helps in the design of optimized oxy-fuel burners.

The main objective of this work was to isolate the role of chemical, thermal and dilution effects of CO_2 on wood burning rate through numerical modeling. Four different mixtures of O_2 and $Ar/CO_2/N_2$ were designed to separate CO_2 effects on wood combustion. Temperature in O_2/CO_2 combustion environment was adjusted to be equal to that of O_2/N_2 environment by adding an appropriate amount of Ar while O_2 amount remained the same. The model was validated by comparing temperature profiles with experimental values. Experiments were done on a laboratory-scale fixed bed.

2. Methodology

2.1 Experimental set-up

A schematic diagram of the experimental set-up used in this work is shown in the Fig. 1. It is a cylindrical burner made of stainless steel which is insulated with refractory cement. A detailed description of the set-up has been given in our previous paper [22].

For all the tests, the burner was filled with wood up to a height of 6 cm. Five type K thermocouples are located at an equidistant of 10 mm from one another. They are connected to a data acquisition system that records temperature every second. Temperature measurement and data acquisition using type K thermocouples were done in accordance to ASTM MNL12 [23]. Combined measurement uncertainty for thermocouple and data acquisition system depends on measured temperature and for the entire range was determined to be between ±2.2 °C and ±6.6 °C. The burner was operated in a batch mode; fuel was fed once while oxidizer was supplied continuously.

2.2 Numerical modeling

Numerical simulations of combustion of wood in the fixed bed were carried out using a commercial software CD-Adapco (STAR CCM+ version 11.04) [24]. Wood burning in a fixed bed was simulated using Lagrange-Euler method, where gas-phase was calculated using computational fluid dynamics, that is, the Euler phase, while solid-phase was tracked in Lagrange phase, using discrete element method. The governing equations of the model are given by Eqs. (1)-(9) and fully described in Ref. [22, 24]:

- Mass conservation equation for gas-phase, Eq. (1) and solid-phase, Eq. (2):

$$\frac{\partial}{\partial t}(\chi\rho_g)+\nabla\cdot(\rho_g\mathbf{v}_g)=\sum\nolimits_{i,g}w_{i,g}^{gs} \tag{1}$$

$$\frac{\partial}{\partial t}\left((1-\chi)\rho_s\right)=\sum\nolimits_{i,s}w_{i,s}^{gs} \tag{2}$$

- Momentum conservation equation for gas-phase, Eq. (3):

$$\frac{\partial}{\partial t}(\chi\rho_g\mathbf{v}_g)+\nabla\cdot(\rho_g\mathbf{v}_g\mathbf{v}_g)=-\nabla p+\nabla\cdot\tau+\rho_g g+S_m \tag{3}$$

where S_m is momentum source term given as;

$$S_m=-\left(\frac{\mu}{c_1}\mathbf{v}_g+C_2\rho_g|\mathbf{v}_g|\mathbf{v}_g\right) \tag{4}$$

- Energy conservation equation for gas-phase, Eqs. (5) and (6) and solid-phase, Eq. (7):

$$\begin{aligned}&\frac{\partial}{\partial t}(\chi\rho_g h_g)+\nabla\cdot(\rho_g\mathbf{v}_g h_g)\\&=\frac{\partial}{\partial t}(\chi p)+\nabla\cdot\left(\lambda_{g,e}\nabla T_g-\sum\nolimits_{i=1}^{N_g}h_{i,g}J_{i,g}\right)+\nabla\cdot(\mathbf{v}_g p)-\nabla\cdot(\tau\cdot\mathbf{v}_g)+S_E\end{aligned} \tag{5}$$

where S_E energy source term given as;

$$S_E=A_s h_c(T_s-T_g)-\sum\nolimits_{i,g}w_{i,g}^{gs}H_{i,g}+q_R \tag{6}$$

$$\begin{aligned}\rho_s c_{ps}(1-\chi)\frac{\partial T_s}{\partial t}=&\nabla\cdot(\lambda_{s,e}\nabla T_s)+A_s h_c(T_g-T_s)+\\&\frac{A_s}{4}Q_{a,p}(G-4\sigma T_s^4)+\sum\nolimits_{i,s}w_{i,s}^{gs}H_{i,s}\end{aligned} \tag{7}$$

- Species conservation equation for gas-phase species *i,g*, Eq. (8) and solid-phase species *i,s*, Eq. (9)

$$\frac{\partial}{\partial t}(\chi\rho_g Y_{i,g})+\nabla\cdot(\rho_g\mathbf{v}_g Y_{i,g})=\nabla\cdot(\rho_g D\nabla Y_{i,g})+w_{i,g}^{gs} \tag{8}$$

Table 1. Proximate and ultimate analyses of fuel sample.

Proximate analysis (wt%)	
Moisture	10.3
Volatile matter (wt% dry basis)	84.9
Fixed carbon (wt% dry basis)	14.9
Ash (wt% dry basis)	0.2
Ultimate analysis (wt% dry basis)	
C	50.87
H	5.73
N	0.3
O (by difference)	43.1
Gross calorific value (MJ/kg)	19.3

Table 2. Physical properties of wood.

Particle size, d_p (m)	0.005
Eucalyptus wood	
Density, ρ (kg/m^3)	1220
Porosity, θ	0.64
Specific heat, c_p (J/kgK)	1500 + T_s
Conductivity, λ_s (W/mK)	0.2
Char	
Density, ρ (kg/m^3)	250
Porosity, θ	0.85
Specific heat, c_p (J/kgK)	420 + 2.09T_s -6.85 × 10^{-4}T_s^2
Conductivity, λ_s (W/mK)	0.1

$$\frac{\partial}{\partial t}\left((1-\chi)\rho_s Y_{i,s}\right) = w_{i,s}^{gs} \tag{9}$$

The symbols are defined in Nomenclature. Exchange of species, mass and energy between the two phases was enabled by a two-way coupling model [22, 24].

Turbulence in both freeboard and bed region was accounted for using standard κ-ε model. Interaction between turbulence and chemistry was solved using eddy dissipation concept. Weighted-sum-of-gray-gas-model (WSGGM) [25], was used as a property model for the radiating gases.

Proximate and ultimate analyses for the samples investigated in this study are presented in Table 1 and physical properties in Table 2. The latter are based on the Mehrabian et al. [26] work.

Chemical kinetics of wood conversion in the bed was simulated using different sub-models, which consisted of drying model, pyrolysis model, homogeneous reaction model and heterogeneous reaction model. Kinetics data of these sub-models are given in Table 3. The rate expressions for these reactions are presented in Table 4. These models were adopted from previous research on wood combustion [27-32]. However, in this work oxy-fuel combustion was accounted for by incorporating a reaction involving CO_2 (R(10)) and its associated chain-branching reactions (R(11) and R(12)) in the homogeneous reaction sub-model. Char combustion rate was evaluated based on partial pressure of O_2, CO_2 and H_2O available at its surface [33]. The stoichiometric ratio of CO_2 to CO from char combustion is dependent on particle surface temperature [27]:

$$\Omega = \frac{2(1+4.3\exp[-3390/T_{particle}])}{2+4.3\exp[-3390/T_{particle}]}. \tag{10}$$

Grid independent solutions were achieved by meshing computational domain into highly-refined unstructured grid as shown in Fig. 2. A quarter of the burner was used for computation since it has a double symmetry. The choice of mesh size was based on a mesh independent test whose results are shown in Fig. 3. The predicted temperature profile at 5 cm from bed bottom under oxy-fuel condition is significantly different when using a mesh that consists of 100000 cells as compared to that of 200000 cells. The difference in temperature profiles is negligible for mesh that consists of 200000, 300000 and 400000 cells, respectively. Therefore, a mesh with 200000 cells was used for all the cases computed.

Oxidizer enters the domain through inlet boundary located at the bottom. The concentration of oxygen and N_2/CO_2/Ar was set in accordance to the required predesigned conditions. In the first set of experiments, O_2 concentration by volume was varied between 21 % and 50 % with diluent as either N_2 or CO_2. In addition, four mixtures were designed to separate the effects of CO_2 environment. The four mixtures were denoted by letters A, B, C and D and their composition by volume was 21 % O_2/79 % N_2; 21 % O_2/22.5 % CO_2/56.5 % Ar; 40 % O_2/60 % CO_2; and 40 % O_2/47 % CO_2/13 % Ar, respectively. The inlet mass flux for the mixture for all the tests was 0.1 kg/m^2/s. The temperature for each of the mixture at the inlet was 295 K. Top boundary was the outlet boundary with temperature and gases concentration gradient set to zero using Neumann boundary condition. A stationary wall with no-slip conditions was considered; the tangential velocity at the wall was explicitly set to zero. The model includes terms to account for heat transfer by radiation and convection at the wall. Emissivity of the surface and coefficient of heat transfer were 0.8 and 10 W/m^2.K, respectively.

3. Results and discussion

Measured temperature profiles at various distances from bed bottom for wood combustion in 21 % oxygen in N_2 and CO_2 are presented in Figs. 4(a) and (b), respectively. The graphs show that the temperature profile at any given height in both environments exhibits similar behavior. They all have two peaks. When the flame front reaches an ignition point, the temperature rises rapidly to the first peak. Then it decreases gradually to another point and finally rises to the second peak.

Combustible pyrolysis products such as CH_4, tar, H_2 and CO are oxidized through exothermic reactions which generate heat, subsequently increasing the temperature. The exothermic

Table 3. Biomass kinetic model.

Drying	Rate expression			Source
R(1) Wet wood → Dry wood + H_2O (g)	$R_{dry} = Y_b \rho_{b,wet} 1.610^{27} \exp(-25000 / T_s)$			[27]
Pyrolysis				
Reaction	$K_i = A_i T^n \exp(-E_i / RT)$			Source
	A_i (s^{-1})	E_i (kJ/mol)	n	
R(2) Dry wood → Gas	111×10^9	177	0	[28]
R(3) Dry wood → Tar	9.28×10^9	149	0	[28]
R(4) Dry wood → Char	30.5×10^9	125	0	[28]
R(5) Tar → $\gamma_t Tar_{inert} + \gamma_{CO} CO + \gamma_{CO2} CO_2 + \gamma_{H2} H_2 + \gamma_{CH4} CH_4$	9.55×10^4	93.37	0	[29, 30]
Homogeneous gas-phase reactions				
Reaction	$K_i = A_i T^n \exp(-E_i / RT)$			Source
	A_i (s^{-1})	E_i (kJ/mol)	n	
R(6) $2CO + O_2 \rightarrow 2CO_2$	2.24×10^{12}	167.36	0	[29, 30]
R(7) $CH_4 + 2O_2 \rightarrow CO_2 + 2H_2O$	11.6×10^{13}	202.5	0	[29, 30]
R(8) $2H_2 + O_2 \rightarrow 2H_2O$	2.19×10^9	109.2	0	[29, 30]
R(9) Tar + $2.9O_2 \rightarrow 6CO + 3.1H_2$	9.2×10^6	80.2	0	[29, 30]
R(10) $CO + OH \rightarrow CO_2 + H$	4.76×10^7	0.293	1.3	[31]
R(11) $H + O_2 \rightarrow O + OH$	2.65×10^{16}	71.347	-0.7	[31]
R(12) $H_2 + O_2 \rightarrow OH + OH$	2.51×10^{12}	163.075	0	[32]
R(13) $H_2O + CO \rightarrow CO_2 + H_2$	2.78	12.55	0	[27, 28]
R(14) $CO_2 + H_2 \rightarrow H_2O + CO$	93.69	46.594	0	[27, 28]
Heterogeneous reactions				
Reaction	$K_i = A_i T^n \exp(-E_i / RT)$			Source
	A_i (s^{-1})	E_i (kJ/mol)	n	
R(15) $\Omega C + O_2 \rightarrow 2(\Omega - 1)CO + (2 - \Omega) CO_2$	2.54×10^{-3}	74.8	0	[29, 30]
R(16) $C + CO_2 \rightarrow 2CO$	1.81×10^{-2}	130	0	[29, 30]
R(17) $C + H_2O \rightarrow CO + H_2$	1.81×10^{-2}	130	0	[29, 30]

Table 4. Rate expression for the reactions.

Reaction	Rate expression	Reaction	Rate expression
R(2)	$w_b = K_2 \rho_{b,dry}$	R(10)	$R_{CO} = K_{10}[CO][OH]$
R(3)	$w_b = K_3 \rho_{b,dry}$	R(11)	$R_H = K_{11}[O][OH]$
R(4)	$w_b = K_4 \rho_{b,dry}$	R(12)	$R_{H2} = K_{12}[H_2][O_2]$
R(5)	$w_{Tar} = K_5 \rho_{Tar}$	R(13)	$R_{H2O} = K_{13}[H_2O][CO]$
R(6)	$R_{CO} = K_6[CO][O_2]^{0.25}[H_2O]^{0.5}$	R(14)	$R_{CO2} = K_{14}[CO_2][H_2]$
R(7)	$R_{CH4} = K_7[CH_4]^{0.7}[O_2]^{0.8}$	R(15)	$w_{char,O2} = K_{15} P_{O2} S_{a,char}$
R(8)	$R_{H2} = K_8[H_2][O_2]$	R(16)	$w_{char,CO2} = K_{16} P_{CO2} S_{a,char}$
R(9)	$R_{Tar} = K_9[Tar]^{0.5}[O_2]$	R(17)	$w_{char,H2O} = K_{17} P_{H2O} S_{a,char}$

reactions occur concurrently with pyrolysis and drying of wood particles, which are endothermic reactions and cause decrease in temperature after the first peak. When pyrolysis and drying processes are completed, exothermic reactions dominate and temperature rises again to the second peak. After the second peak, the temperature gradually decreases until the end of combustion. During this phase, a wood particle has completely been devolatilized, leaving a pure char that undergoes oxidation and gasification with H_2O and CO_2. It is deduced that gasification, which is endothermic, is more pronounced than exothermic process (oxidation), hence the temperature decrease.

Figs. 4(a) and (b) also show that at corresponding height, air-fuel peak temperature is higher than oxy-fuel temperature by about 200 K. This is a result of the combination of both chemical and thermal effects. Lower temperatures are seen in

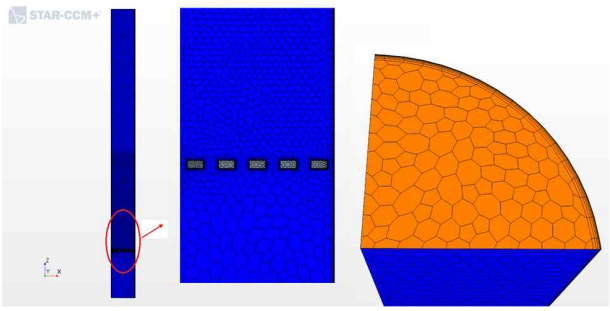

Fig. 2. Computational mesh for the fixed bed: (a) Highly refined mesh in fuel bed and grate; (b) prismatic layers near the wall.

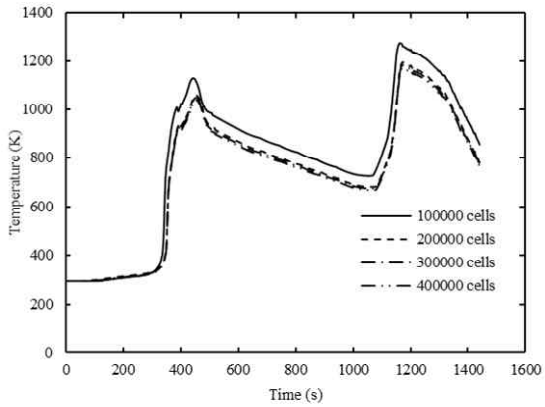

Fig. 3. Predicted temperature profiles at 5 cm from the bed bottom for wood combustion in 21 % O_2/79 % CO_2 mixture for different mesh sizes.

oxy-fuel environment because CO_2 has higher heat capacity than N_2. Furthermore, chemical effect through endothermic reaction of CO_2 with char contributes in lowering the temperature of oxy-fuel environment.

The individual contribution of various effects of CO_2, namely, chemical, thermal and oxygen concentration effects are evaluated through CFD-DEM modeling. The model results are validated by comparing them with experimental values. Shown in Fig. 5 are measured and predicted temperature profiles at 5 cm from bed bottom for air-fuel and oxy-fuel environments both at 21 % O_2 concentration. The accuracy of model data was good with deviation of most points from measured values being within 10 %.

Presented in Fig. 6 are predicted temperature profiles at 5 cm from the bed bottom for wood combustion in different combustion atmospheres. It is observed that peak temperature occurrence time comes much earlier in N_2 atmosphere than in CO_2 atmosphere. This is an indication that combustion rate is slower in CO_2 environment. For oxy-fuel combustion, peak temperature value is directly proportional to O_2 concentration. In addition, its occurrence time increases as O_2 concentration is decreased. Peak temperature of oxy-fuel atmosphere, which is equivalent to that of standard air-fuel condition, occurs at about 40 % O_2 concentration. However, its occurrence time is

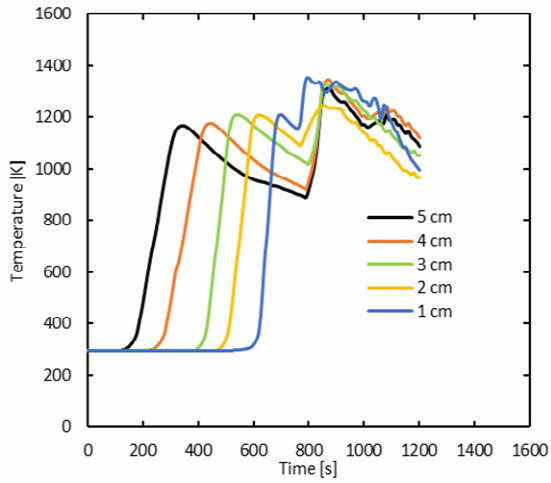

(a) 21 % O_2/79 % N_2 mixture

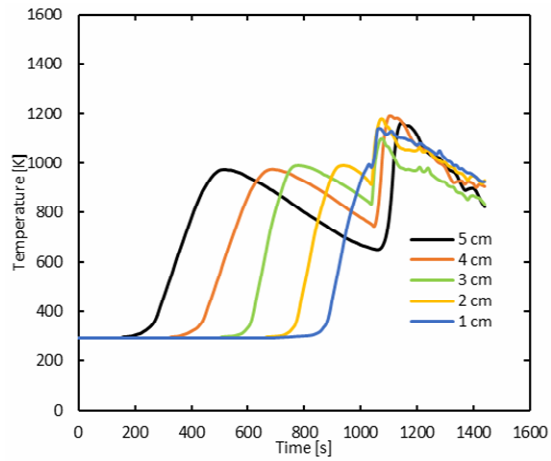

(b) 21 % O_2/79 % CO_2 mixture

Fig. 4. Measured temperature profiles at various distances from the bed bottom for wood combustion in different combustion atmospheres.

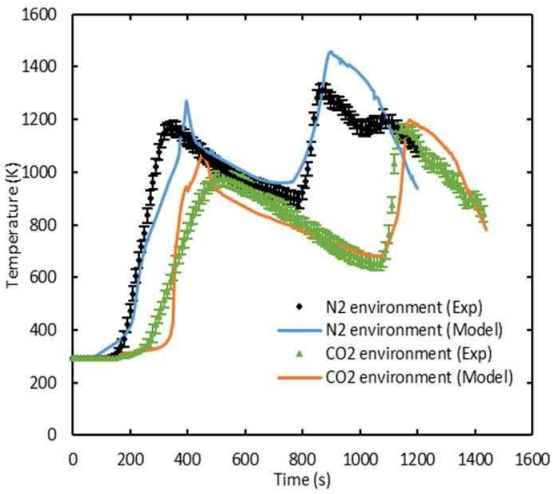

Fig. 5. Measured and predicted temperature profiles at 5 cm from the bed bottom for wood combustion in 21 % O_2/79 % N_2 and 21 % O_2/79 % CO_2 mixtures. Error bars are the standard deviations.

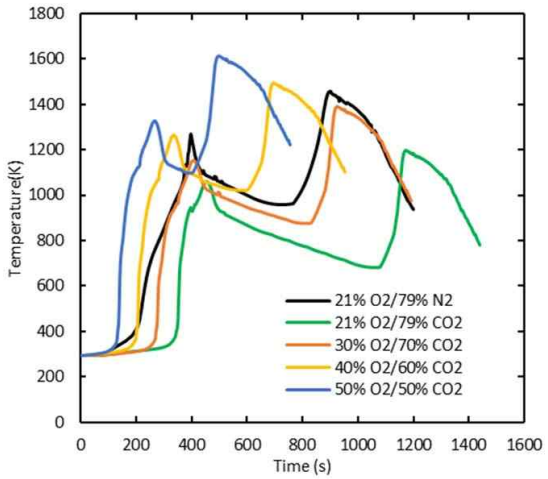

Fig. 6. Predicted temperature profiles at 5 cm from the bed bottom for wood combustion in different combustion atmospheres.

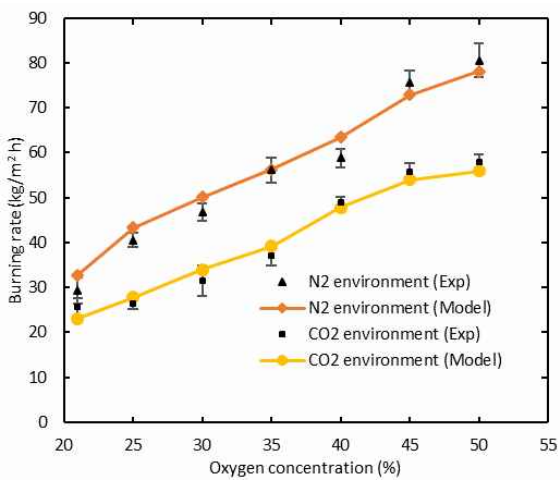

Fig. 8. Measured and predicted burning rates for fuel bed of wood combustion in N_2 and CO_2 environments. Error bars are the standard deviations.

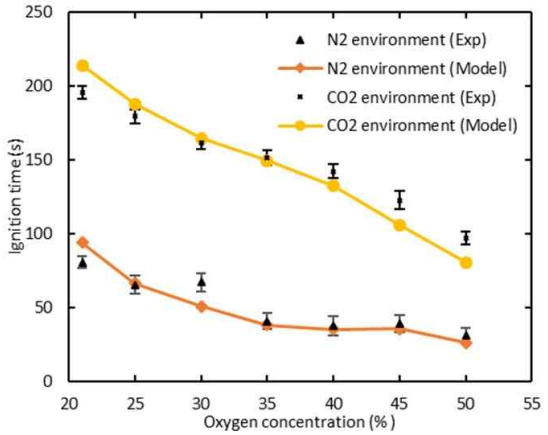

Fig. 7. Measured and predicted ignition time for fuel bed of wood combustion in N_2 and CO_2 environments. Error bars are the standard deviations.

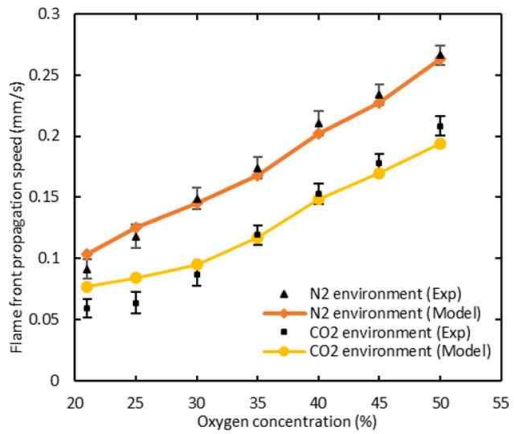

Fig. 9. Measured and predicted flame front propagation speed for fuel bed of wood combustion in N_2 and CO_2 environments. Error bars are the standard deviations.

slightly earlier than in air-fuel condition.

The time taken for the reaction front to start at the top surface of the fuel bed was defined as ignition time. Presented in Fig. 7 is ignition time for wood combustion in both oxy-fuel and air-fuel environments. The graph shows that at any given oxygen concentration, ignition time in oxy-fuel environment is almost twice that of corresponding air-fuel condition. Retarded ignition in CO_2 environment could be attributed to its high specific heat capacity and low O_2 diffusivity in it. In both cases, ignition time gradually decreases as oxygen concentration is increased.

A comparison of burning rates for wood combustion in N_2 and CO_2 burning conditions is presented in Fig. 8. At the same O_2 concentration, the burning rate in CO_2 burning atmosphere is less than in N_2 burning atmosphere. The burning rate of wood particles in oxy-fuel condition is lowered by the aforementioned CO_2 effects, which contribute differently as will be discussed later. Thermal diffusivity of CO_2 is less than that of N_2 by about 35 % [34]. In addition, CO_2 absorbs radiative heat more than N_2. The overall effect of these thermal properties of CO_2 is a decrease in burning rate as seen in Fig. 8. Furthermore, the burning rate in oxy-fuel environment is also decreased by chemical effect of CO_2 through Boudouard reaction R(16), which is endothermic. On the other hand, the role played by dilution is clearly demonstrated in Fig. 8. In both cases, burning rate is directly proportional to O_2 concentration. More O_2 concentration enhances oxidation of combustible pyrolysis products and char, hence releasing more heat and increases the burning rates.

Illustrated in Fig. 9 is the flame front propagation speed for wood combustion in oxy-fuel and air-fuel burning atmospheres. For all oxygen concentrations, CO_2 burning atmosphere had lower propagation speed as compared to N_2 burning atmosphere. Furthermore, as oxygen concentration increased flame propagation speed also increased. Flame speed is directly linked to the burning rate. Therefore, the factors which

reduce the burning rates in oxy-fuel environment as discussed in the preceding paragraph are also responsible for the reduced flame speed.

The species and temperature profiles along axial length of the fixed bed when the flame front is at 4 cm from the grate for 21 % O_2/79 % CO_2, 30 % O_2/70 % CO_2, 40 % O_2/60 % CO_2 and 50 % O_2/50 % CO_2 are presented in Figs. 10(a)-(d). The flame structures are similar in profile but differ in magnitude. The flame front for the mixture with high O_2 concentration, 50 %, reaches 4 cm plane at 191 s, which is earlier than those for 40 %, 30 % and 21 % that reached the plane at 275 s, 360 s and 482 s, respectively. This is because flame speed increases as O_2 concentration is increased. As shown in Figs. 10(a)-(d) and Table 5, the amount of tar and CH_4 is high at the reaction zone of 21 % O_2 concentration mixture and decreases gradually for 30 %, 40 % and 50 % O_2 concentration mixtures. The graphs show that the mixture with 21 % O_2 concentration is operating under fuel rich conditions and does not have enough O_2 to oxidize these species through reactions R(7) and R(9). On the other hand, the graphs show that the mixtures with 30 %, 40 % and 50 % O_2 concentration are operating under fuel lean conditions and have excess O_2 in their reaction zones. Thus, reduced amount of tar and CH_4 are observed in these mixtures as compared to those of 21 % O_2 concentration mixture. Consequently, since these reactions are exothermic, a high amount of heat is released as O_2 concentration is increased. This is seen in the peak temperatures attained by these mixtures, Fig. 6. The high amount of heat released increases the heating rates for the particles in the bed and explains the higher flame front propagation speed and burning rates for high O_2 concentration mixtures. High heat energy also accelerates the ignition of the particles for mixtures with high O_2 concentration.

Figs. 10(a)-(d) and Table 5 show that the amount of CO is highest in the reaction zone of the mixture with 30 % O_2 concentration. The mixtures with 21 %, 40 % and 50 % O_2 concentration have almost the same amount of CO in their reaction zone. Unlike tar and CH_4 whose sole source is devolatilization of the wood particles, CO is produced from devolatilization process, oxidation of tar through reaction R(9) and char gasification with CO_2 through reaction R(16). CO is consumed by oxidation reaction R(6). For a mixture with high O_2 concentration, excess O_2 brings an antagonistic effect to the amount of CO where there is a tendency for high consumption through oxidation reaction R(6) and high production by oxidation of tar through reaction R(9) as compared to that of a mixture with low O_2 concentration. However, for mixtures with high O_2 concentration, the production of CO through char gasification could be less than that of low O_2 concentration mixture because of low amount of CO_2. The overall effect of these reactions is that there is an increase in CO production as O_2 concentration is increased up to a peak point, then it starts to decrease.

Burning rate, ignition of fuel particles and flame front propagation speed are all influenced by thermal behavior of

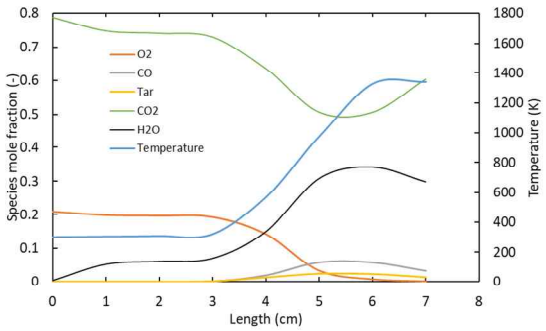

(a) 21 % O_2/79 % CO_2 mixture

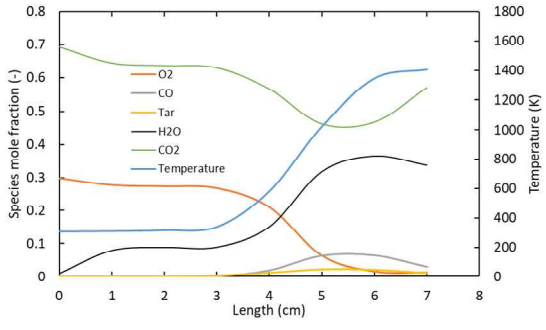

(b) 30 % O_2/70 % CO_2 mixture

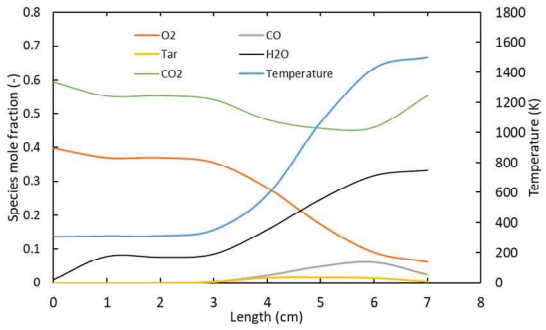

(c) 40 % O_2/60 % CO_2 mixture

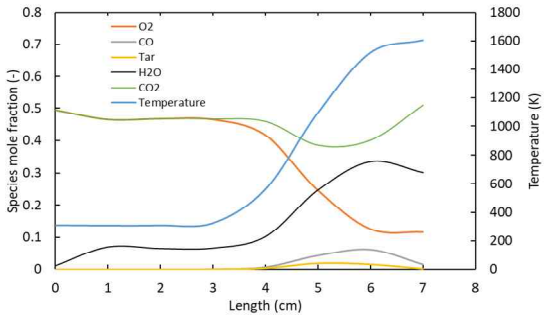

(d) 50 % O_2/50 % CO_2 mixture

Fig. 10. Species and temperature profiles along axial length of the bed for different O_2/CO_2 mixtures when the flame front is at 4 cm from the grate.

the bed. Apart from heat of combustion through chemical reactions discussed in the preceding paragraphs, flame temperature at a given point is also determined by heat flux distribution in the bed, which is mostly by radiation. H_2O and CO_2 are the main products of combustion that participate in radia-

Table 5. Peak values of major combustible species and temperature profiles for wood combustion in different O_2/CO_2 mixtures.

Temperature/ species mole fraction (-)	O_2/CO_2 mixture			
	21 % O_2	30 % O_2	40 % O_2	50 % O_2
Temperature (K)	1338	1406	1499	1605
Tar	0.02427	0.02164	0.01605	0.01837
CO	0.05839	0.06488	0.06013	0.06124
CH_4	0.00819	0.00769	0.00542	0.00684

tion. The presence of high amount of CO_2 in an oxy-fuel environment makes it more emissive than air-fuel environment. As depicted by the flame temperatures in Figs. 6 and 10, a large amount of heat energy is released in the fuel bed with a high O_2 concentration mixture. In this study, the heat energy contribution from different sources has not been separated. Therefore, an increase in heat energy cannot be explicitly linked to a particular source. Though, in the region of intense combustion, heat contributed by combustion is more dominant; the contribution by radiation heat flux is only 10-15 % [35].

Wood combustion in four different mixtures of O_2 and $Ar/CO_2/N_2$ was numerically simulated so as to separate the various effects of CO_2 on burning rate of wood. For all the cases, temperature profiles at 5 cm from fuel bed were considered. A method of adjusting the flame temperature using Ar, which was initially proposed by Du et al. [15] and previously used by other researchers [14, 16, 17], was implemented in this study. The compositions of the four mixtures are specified in Sec. 2.2. Furthermore, other properties of the different mixtures such as mass fraction of the constituents, combined heat capacity and oxygen diffusion coefficient are provided in Table 6. These properties were evaluated and compared at room temperature (298 K), ignition temperature (500 K) and flame temperature (1400 K). Combustion of wood in mixtures A, B and C was designed to have the same peak temperatures, as shown in Fig. 11. A large amount of Ar in mixture B was to increase the peak temperature, which is low when CO_2 alone is used as a diluent. As shown in Table 6, this mixture has a lower specific heat capacity. This enabled the mixture to have the same peak temperature as that of mixture A and C. The peak temperature of wood combustion in mixture D was higher than for the other three by 167 K.

The burning rates of wood combustion in the four mixtures were evaluated and presented in Fig. 12. Burning rate in mixture A was used as a datum. The difference in burning rates of combustion in mixture A and B is due to chemical effect because they have the same oxygen concentration and temperature values. Since temperature is the only similar parameter for combustion in mixture A and C, then the difference in their burning rate is due to a combination of oxygen concentration and chemical effect. Oxygen concentration effect is achieved when oxygen concentration is increased to 40 % while maintaining the same temperature in CO_2 environment (combus-

Table 6. Composition, combined heat capacity and O_2 diffusion coefficient of the four mixtures at different temperatures.

Properties		Gas mixtures			
		A	B	C	D
Mass fraction of components (-)	O_2	0.233	0.171	0.327	0.331
	CO_2	0.000	0.253	0.673	0.535
	N_2	0.767	0.000	0.000	0.000
	Ar	0.000	0.576	0.000	0.134
c_p for the mixture (kJ/kg K)	At 298 K	1.005	0.670	0.868	0.825
	At 500 K	1.030	0.725	1.006	0.939
	At 1400 K	1.209	0.826	1.255	1.147
O_2 diffusion coefficient in the mixture (cm^2/s)	At 298 K	0.209	0.184	0.156	0.164
	At 500 K	0.513	0.462	0.398	0.415
	At 1400 K	2.888	2.642	2.310	2.401

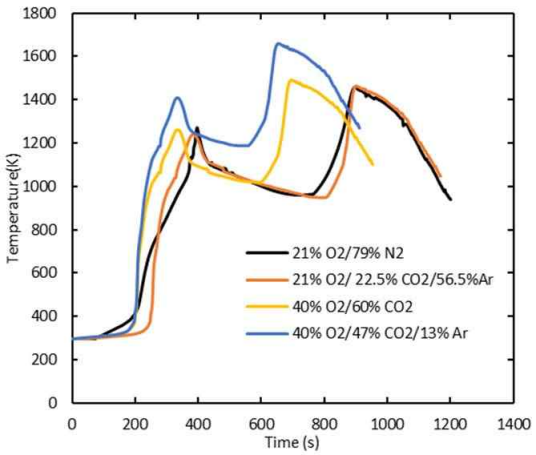

Fig. 11. Predicted temperature profiles at 5 cm from the bed bottom for wood combustion in four combustion environments.

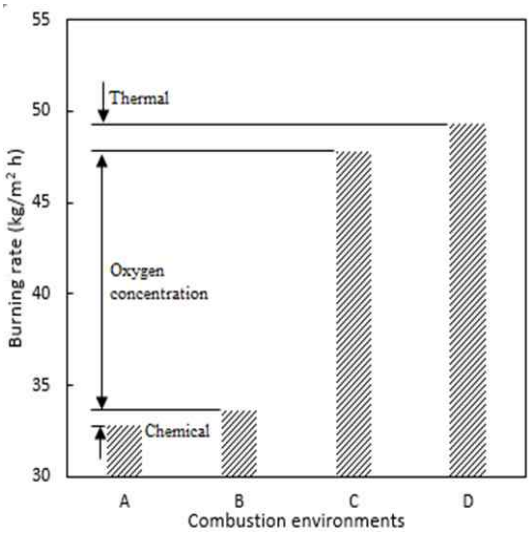

Fig. 12. Predicted separate effects of CO_2 on burning rates for wood combustion in four combustion environments.

tion in mixture B and C). Finally, the difference in burning rates for combustion in mixture C and D is due to thermal effect since they have the same oxygen concentration but different temperature values.

The individual contribution of CO_2 effects on burning rates of wood combustion is evaluated from Fig. 12. It was established that chemical, thermal and oxygen concentration influenced burning rate of wood by 5 %, 9 % and 86 %, respectively. It is evident that oxygen concentration is the most influential parameter in the burning rate. As oxygen concentration is increased, oxidation of char and combustible pyrolysis products is also enhanced. Therefore, more heat is generated and fuel burning rate is significantly improved. The influence of thermal and chemical is not very significant. Thermal effect is only 9 % and translate to a temperature change of 167 K. Chemical effect on the burning rate is quite small because the rate of the chemical reactions involving CO_2 consumption (R(14) and R(16)) is far much less compared to the rate of (R(6) and R(13)).

4. Conclusions

The overall and separate effects of CO_2 burning atmosphere on the combustion properties of wood burning in a fixed bed were investigated through numerical modeling. Modeling was validated by comparison with measured data. The following are the key findings:

- The dilution effect is the most influential parameter on the burning rate of wood combustion in an oxy-fuel system. The influence of thermal and chemical is not very significant.
- Peak temperature of oxy-fuel atmosphere, which is equivalent to that of standard air-fuel condition, occurs at a higher O_2 concentration. However, its occurrence time is slightly earlier than in air-fuel condition.
- At any given oxygen concentration, ignition time in oxy-fuel is almost twice that of corresponding air-fuel condition. In both cases, ignition time gradually decreases as oxygen concentration is increased.
- At the same oxygen concentration, burning rate and flame propagation speed in CO_2 combustion environment was less than in N_2 combustion environment.

Acknowledgments

This work was financially supported by both Dedan Kimathi University of Technology, Kenya and Technische Hochschule Wildau, Germany. The first Author would like to thank German Academic Exchange Service (DAAD) for the financial support for his stay in Technische Hochschule Wildau, Germany.

Nomenclature

A : Arrhenius pre-exponent factor [s^{-1} (mol m^{-3})]
A_s : Particle surface area [m^2]
c_p : Specific heat [J kg^{-1} K^{-1}]
C_1 : Permeability [m^2]
C_2 : Inertia loss coefficient [m^{-1}]
CFD : Computation fluid dynamics
d : Particle diameter [m]
D : Diffusivity [m^2 s^{-1}]
DEM : Discrete element method
E : Activation energy [J mol^{-1}]
g : Gravity [m s^{-2}]
G : Incident radiative heat flux [W m^{-2}]
h : Enthalpy [J kg^{-1}]
h_c : Convective heat transfer coefficient [W m^{-2} K^{-1}]
H_i : Enthalpy of formation of species i [J kg^{-1}]
J : Diffusion mass flux [kg m^{-2} s^{-1}]
K : Rate constant [s^{-1} (mol m^{-3})]
N_g : Number of gas species [-]
p : Pressure [Pa]
q_R : Radiative heat flux [W m^{-2}]
$Q_{a,p}$: Particle absorption coefficient [-]
R : Universal gas constant [J mol^{-1} K^{-1}]
S_a : Specific surface area [m^{-1}]
S_E : Energy source term [J m^{-3} s^{-1}]
S_M : Momentum source term [kg m^{-2} s^{-2}]
t : Time [s]
T : Temperature [K]
v : Velocity [m s^{-1}]
w_i : Rate of production of species I [kg m^{-3} s^{-1}]
WSGGM : Weighted-sum-of-gray-gas-model
Y : Mass fraction [-]

Greek symbols

ε : Turbulent dissipation rate [J kg^{-1} s^{-1}]
θ : Particle porosity [-]
κ : Turbulent kinetic energy [J kg^{-1} s^{-1}]
λ : Thermal conductivity [W m^{-1} K^{-1}]
μ : Viscosity [kg m^{-1} s^{-1}]
ρ : Density [kg m^{-3}]
σ : Stefan-Boltzmann constant [W m^{-2} K^{-4}]
τ : Shear stress tensor [Pa]
χ : Region porosity [-]
Ω : Stoichiometric coefficient [-]

Subscripts

b : Biomass
e : Effective
g : Gas
i : i^{th} reaction
i,g : Gaseous species
i,s : Solid-phase species
p : Particle
s : Solid

Superscript

gs : Heterogeneous reaction
n : Exponent

Operators

∇ : Gradient operator
$\nabla\cdot$: Divergence operator

References

[1] International Energy Agency, *World Energy Outlook 2016: Executive Summary*, https://www.iea.org (2016).

[2] S. K. Hong, D. S. Noh and J. B. Yang, Experimental study of honeycomb regenerator system for oxy-fuel combustion, *J. of Mechanical Science and Technology*, 27 (4) (2013) 1151-1154.

[3] S. H. Tak, S. K. Park, T. S. Kim, J. L. Sohn and Y. D. Lee, Performance analyses of oxy-fuel power generation systems including CO_2 capture: Comparison of two cycles using different recirculation fluids, *J. of Mechanical Science and Technology*, 24 (9) (2010) 1947-1954.

[4] D. Kim and S. Choi, Effect of typical modeling assumptions for pulverized coal char combustion commonly used in commercial CFD codes, *J. of Mechanical Science and Technology*, 29 (11) (2015) 4951-4961.

[5] R. Ben-Mansour, P. Ahmed, M. A. Habib and A. Jamal, Oxy-combustion of liquid fuel in an ion transport membrane reactor, *International J. of Energy and Environmental Engineering*, 9 (2018) 21-37.

[6] R. Marsh, J. Runyon, A. Giles, S. Morris, D. Pugh, A. Valera-Medina and P. Bowen, Premixed methane oxy-combustion in nitrogen and carbon dioxide atmospheres: Measurement of operating limits, flame location and emissions, *Proceedings of the Combustion Institute*, 36 (3) (2017) 3949-3958.

[7] G. Scheffknecht, L. Al-Makhadmeh, U. Schnell and J. Maier, Oxy-fuel coal combustion - A review of the current state-of-the-art, *International J. of Greenhouse Gas Control*, 5 (2011) 16-35.

[8] J. Ahn, H. J. Kim and K. S. Choi, Oxy-fuel combustion boiler for CO_2 capturing: 50 kW-class model test and numerical simulation, *J. of Mechanical Science and Technology*, 24 (10) (2010) 2135-2141.

[9] S. K. Hong, K. G. Kang, D. S. Noh, E. K. Lee and H. S. Ryou, Development of an oxy-fuel combustor with fuel preheating for regenerator system, *J. of Mechanical Science and Technology*, 29 (10) (2015) 4555-4559.

[10] S. Park, J. A. Kim, C. Ryu, W. Yang, Y. J. Kim and S. Seo, Effects of gas and particle emissions on wall radiative heat flux in oxy-fuel combustion, *J. of Mechanical Science and Technology*, 26 (5) (2012) 1633-1641.

[11] A. Molina and C. R. Shaddix, Ignition and devolatilization of pulverized bituminous coal particles during oxy-gen/carbon dioxide coal combustion, *Proceedings of the Combustion Institute*, 31 (2) (2007) 1905-1912.

[12] J. Riaza, M. V. Gil, L. Álvarez, C. Pevida, J. J. Pis and F. Rubiera, Oxy-fuel combustion of coal and biomass blends, *Energy*, 41 (1) (2012) 429-435.

[13] L. Álvarez, C. Yin, J. Riaza, C. Pevida, J. J. Pis and F. Rubiera, Biomass co-firing under oxy-fuel conditions: A computational fluid dynamics modelling study and experimental validation, *Fuel Processing Technology,* 120 (2014) 22-33.

[14] Q. Wang, G. Legros, J. Bonnety and C. Morin, Experimental characterization of the different nitrogen dilution effects on soot formation in ethylene diffusion flames, *Proceedings of the Combustion Institute*, 36 (2) (2017) 3227-3235.

[15] D. X. Du, R. L. Axelbaum and C. K. Law, The influence of carbon dioxide and oxygen as additives on soot formation in diffusion flames, *Symposium (International) on Combustion/The Combustion Institute*, 23 (1) (1990) 1501-1507.

[16] K. Al-Qurashi, A. D. Lueking and A. L. Boehman, The deconvolution of the thermal, dilution, and chemical effects of exhaust gas recirculation (EGR) on the reactivity of engine and flame soot, *Combustion and Flame*, 158 (9) (2011) 1696-1704.

[17] Y. Zhou, X. Jin and Q. Jin, Numerical investigation on separate physicochemical effects of carbon dioxide on coal char combustion in O_2/CO_2 environments, *Combustion and Flame*, 167 (2016) 52-59.

[18] F. Shan, Q. Lin, K. Zhou, Y. Wu, W. Fu, P. Zhang, L. Song, C. Shao and B. Yi, An experimental study of ignition and combustion of single biomass pellets in air and oxy-fuel, *Fuel*, 188 (2017) 277-284.

[19] J. Riaza, R. Khatami, Y. A. Levendis, L. Álvarez, M. V. Gil, C. Pevida, F. Rubiera and J. J. Pis, Single particle ignition and combustion of anthracite, semi-anthracite and bituminous coals in air and simulated oxy-fuel conditions, *Combustion and Flame*, 161 (4) (2014) 1096-1108.

[20] J. G. Pohlmann, E. Osório, A. C. F. Vilela, M. A. Diez and A. G. Borrego, Pulverized combustion under conventional (O_2/N_2) and oxy-fuel (O_2/CO_2) conditions of biomasses treated at different temperatures, *Fuel Processing Technology,* 155 (2017) 174-182.

[21] M. V. Gil, J. Riaza, L. Álvarez, C. Pevida, J. J. Pis and F. Rubiera, Kinetic models for the oxy-fuel combustion of coal and coal/biomass blend chars obtained in N_2 and CO_2 atmospheres, *Energy*, 48 (1) (2012) 510-518.

[22] J. K. Tanui, P. N. Kioni, T. Mirre and M. Nowitzki, The effect of carbon dioxide on flame propagation speed of wood combustion in a fixed bed under oxy-fuel conditions, *Fuel Processing Technology,* 179 (2018) 285-295.

[23] R. M. Park, R. M. Carroll, P. Bliss, G. W. Burns, R. R. Desmaris, F. B. Hall, M. B. Herzkovitz, D. MacKenzie, E. F. McGuire, R. P. Reed, L. L. Sparks and T. P. Wang (eds.), *ASTM MNL12 - Manual on the Use of Thermocouples in Temperature Measurement*, Fourth Ed., Sponsored by

ASTM Committee E20 on Temperature Measurement, West Conshohocken, USA (1993).
[24] CD-Adapco, *STAR CCM+ Version 11.04*, www.cd-adapco.com (2017).
[25] T. F. Smith, Z. F. Shen and J. N. Friedman, Evaluation of coefficients for the weighted sum of gray gases model, *J. Heat Transf.,* 104 (4) (1982) 602-608.
[26] R. Mehrabian, A. Shiehnejadhesar, R. Scharler and I. Obernberger, Multi-physics modelling of packed bed biomass combustion, *Fuel*, 122 (2014) 164-178.
[27] R. Johansson, H. Thunman and B. Leckner, Influence of intraparticle gradients in modeling of fixed bed combustion, *Combustion and Flame*, 149 (2007) 49-62.
[28] M. Gómez, J. Porteiro, D. de la Cuesta, D. Patiño and J. Míguez, Numerical simulation of the combustion process of a pellet-drop-feed boiler, *Fuel*, 184 (2016) 987-999.
[29] A. H. Mahmoudi, M. Markovic, B. Peters and G. Brem, An experimental and numerical study of wood combustion in a fixed bed using Euler-Lagrange approach (XDEM), *Fuel*, 150 (2015) 573-582.
[30] A. H. Mahmoudi, F. Hoffmann, M. Markovic, B. Peters and G. Brem, Numerical modeling of self-heating and self-ignition in a packed-bed of biomass using XDEM*, Combustion and Flame*, 163 (2016) 358-369.
[31] G. P. Smith, D. M. Golden, M. Frenklach, N. W. Moriarty, B. Eiteneer, M. Goldenberg, C. T. Bowman, R. K. Hanson, S. Song, W. C. Gardiner Jr., V. V. Lissianski and Z. Qin, *GRI-MECH 3.0*, http://www.me.berkeley.edu/gri_mech/ (1999).
[32] C. K. Westbrook and F. L. Dryer, Chemical kinetic modeling of hydrocarbon combustion, *Prog. Energy Combust. Sci*., 10 (1) (1984) 1-57.
[33] D. D. Evans and H. W. Emmons, Combustion of wood charcoal, *Fire Research*, 1 (1977) 57-66.
[34] T. Suda, K. Masuko, J. Sato, A. Yamamoto and K. Okazaki, Effect of carbon dioxide on flame propagation of pulverized coal clouds in CO_2/O_2 combustion, *Fuel,* 86 (2007) 2008-2015.
[35] N. Lallemant, A. Sayre and R. Weber, Evaluation of emissivity correlations for H_2O-CO_2-N_2/air mixtures and coupling with solution methods of the radiative transfer equation, *Prog. Energy Combust. Sci*., 22 (6) (1996) 543-574.

J. K. Tanui received his B.Sc. and M.Sc. in Mechanical Engineering from Jomo Kenyatta University of Agriculture and Technology (JKUAT), Nairobi, Kenya, in 2009 and 2013, respectively. He is currently doing his Ph.D. at Dedan Kimathi University of Technology (DeKUT) with special arrangements to carry out some research at Technische Hochschule Wildau, Germany. His research interests include combustion and gasification of solid fuels, biofuels combustion and kinetics, emissions and pollutant formation in fuels.

P. N. Kioni received his B.Sc. in Mechanical Engineering from University of Nairobi, Kenya, in 1988, and Ph.D. from Cambridge University, United Kingdom, in 1994. He is a Professor of Mechanical Engineering at DeKUT. His research interests include studies of reacting flows.

T. Mirre received his Dipl.-Ing. in power plant technology and transformation of energy, special nuclear technology from Technical University Zittau in 1982. In 1992 he became a Professor in the Faculty of Mechanical Engineering at the University of Applied Science (UAS) Wildau and from 1998 to 2010 he was the Dean of the faculty. His subject area is thermodynamics, flows and turbo-engines.

M. Nowitzki received his Dipl.-Ing. in Process Engineering from UAS Wildau in 2005. He is currently working at UAS Wildau and doing his Dr.-Ing. at the Brandenburg University of Technology Cottbus-Senftenberg. His research interests include multiphase flow simulation, Tesla microturbines, substance transition in rectification columns and heat transfer.